Oceanic spreading center–hotspot interactions: Constraints from along-isochron bathymetric and gravity anomalies

Garrett Ito Woods Hole Oceanographic Institution–Massachusetts Institute of Technology Joint Program in Oceanography, Woods Hole, Massachusetts 02543
Jian Lin Woods Hole Oceanographic Institution, Woods Hole, Massachusetts 02543

ABSTRACT

We analyzed bathymetric and gravity anomalies along present and paleoaxes of oceanic spreading centers influenced by the Iceland, Azores, Galápagos, Tristan, and Easter hotspots. Residual bathymetry (up to 4.7 km) and mantle Bouguer gravity (up to −340 km) anomalies are maximum at on-axis hotspots and decrease with increasing ridge-hotspot separation distance *(D),* until becoming insignificant at $D \sim 500$ km. Along-isochron widths of bathymetric anomalies (up to 2700 km) depend inversely on paleo–spreading rate, reflecting the extent to which plume material will flow along axis before being swept away by the spreading lithosphere. Flux balance arguments suggest that the five hotspots feed material to ridges with comparable fluxes of $\sim 2.2 \times 10^6$ km^3/m.y. Assuming that the amplitudes of these geophysical anomalies reflect temperature-dependent crustal thickness and mantle density variations, we suggest that ridge temperature anomalies are maximum (150–225 C) when plumes are ridge centered and decrease with increasing ridge-hotspot distance due to cooling of the ridgeward-migrating plume material.

INTRODUCTION

When mantle plumes rise near oceanic spreading centers, they generate not only near-ridge hotspots, but also melt anomalies at the axis of the nearby ridges (e.g., Morgan, 1978). Direct evidence that near-ridge plumes divert toward and feed ridges is the ocean-island basalt (OIB) geochemical signature in ridge basalts (e.g., Hart et al., 1973). Furthermore, along-axis gradients in the strength of OIB signatures and in topography (e.g., Vogt, 1976; Schilling, 1991) indicate that once a plume reaches a ridge, it spreads laterally along axis.

Previous studies of ridge-plume interactions have focused primarily on present-day spreading centers. Ito and Lin (1995), however, demonstrated that 70%–75% of off-axis bathymetric and gravity anomalies of the Cocos plate can be attributed to the anomalous crustal thicknesses generated at the paleo-Galápagos ridge axis. We attributed long-wavelength (>200 km) variations in bathymetry and gravity along crustal isochrons to temperature conditions beneath the hotspot-influenced ridge axis at the time the crust was created.

In this study we investigated the evolution of five prominent plume-ridge systems over wide ranges in ridge-hotspot separation distance and spreading rate. The results of this study provide observational constraints on the amplitudes of along-isochron bathymetric and gravity anomalies as they depend on ridge-hotspot separation distance, and along-isochron widths of bathymetric anomalies as they depend on ridge spreading rate.

ALONG-ISOCHRON BATHYMETRIC AND GRAVITY ANOMALIES

Iceland, Azores, Tristan, Galápagos, and Easter (Fig. 1) are the five hotspots that impose the most prominent bathymetric and geo-

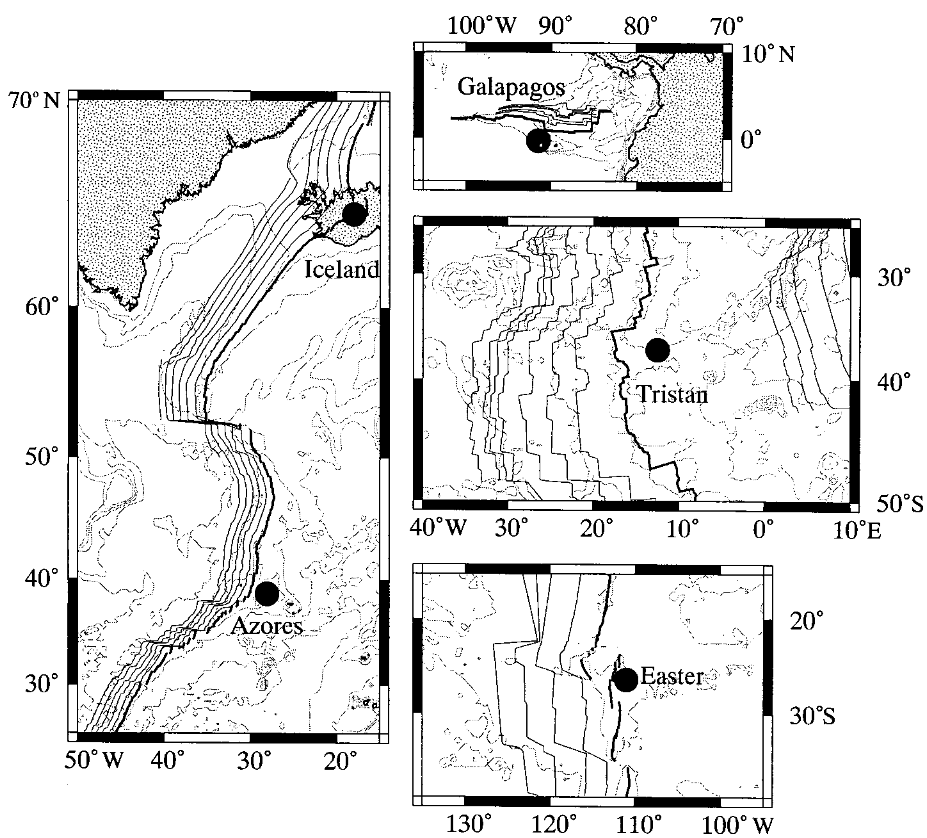

Figure 1. Regional bathymetric maps (mercator projections) of five prominent hotspot-ridge systems: Iceland, Azores, and Tristan, near Mid-Atlantic Ridge; Galápagos, near Galápagos spreading center; and Easter, near East Pacific Rise. Etopo5 (Earth topography at 5 minute grid spacing, National Geophysical Data Center Report MGG-5) bathymetry points within 5 min of ship data points were omitted before gridding at 5 min grid spacing. Circles mark present-day locations of hotspots; solid lines mark ridge axes and off-axis isochrons along which data profiles were taken. To exclude sea floor affected by off-axis volcanism we used isochrons of ages 0–30 Ma for Iceland and 0–25 Ma for Azores on North American plate; 0–8 Ma for Galápagos on Cocos plate; and 0–20 Ma for Easter on Pacific plate. For Tristan, we used isochrons of ages 0–70 Ma on South American plate and ages 80–110 Ma on African plate because hotspot crossed from South American to African plate at ~80 Ma (O'Connor and Duncan, 1990).

chemical anomalies observed at nearby oceanic spreading centers (Hart et al., 1973; Hamelin et al., 1984; Schilling, 1985). Encompassing each of the five systems, we obtained shipboard bathymetric data from the National Geophysical Data Center (NGDC) and Lamont-Doherty Earth Observatory (LDEO), and gridded bathymetry from NGDC. To derive residual bathymetry, we first corrected the raw data for isostatic effects of sediment loading and then subtracted predicted depths of a cooling mantle half space (Carlson and Johnson, 1994). Sediment thicknesses were obtained from the LDEO database (A. Cazenave, Centre National d'Etudes Spatiales, Toulouse, France), and density contrasts between the sediments and mantle, and mantle and water were assumed to be 1600 kg/m^3 and 2300 kg/m^3, respectively.

Free-air gravity data were taken from the ship surveys and the satellite altimetry-derived gravity grid of Sandwell and Smith (1992). To isolate the effects of sub–sea-floor density structure, we generated mantle Bouguer anomalies by subtracting from the free-air gravity the attractions of the sea-floor–water (density contrast, $\Delta\rho$ = 1800 kg/m^3) and crust-mantle ($\Delta\rho$ = 500 kg/m^3) interfaces using raw bathymetry, and assuming a crust of uniform thickness (6.5 km) (e.g., Kuo and Forsyth, 1988).

Coordinates of present-day ridge axes and crustal isochrons were defined by using plate boundary and age data of Müller et al. (1993a). Because our focus was on anomalies generated at the axes of spreading centers, we considered only data from sea floor unaffected by off-axis volcanism, as detailed in the Figure 1 caption. From our residual bathymetry and mantle Bouguer grids, we then extracted along-isochron profiles (Fig. 2).

ANOMALY AMPLITUDES VS. PALEORIDGE-HOTSPOT DISTANCE

To determine hotspot locations relative to paleo–spreading centers, we assumed that the hotspots were stationary with respect to each other and used plate-reconstruction poles (Lonsdale 1988; Müller et al., 1993b) to rotate isochrons with respect to the hotspots back to their positions at the time of accretion. We then measured distances between the paleo–ridge axes and hotspot centers, which we took to be the locations of most recent volcanism.

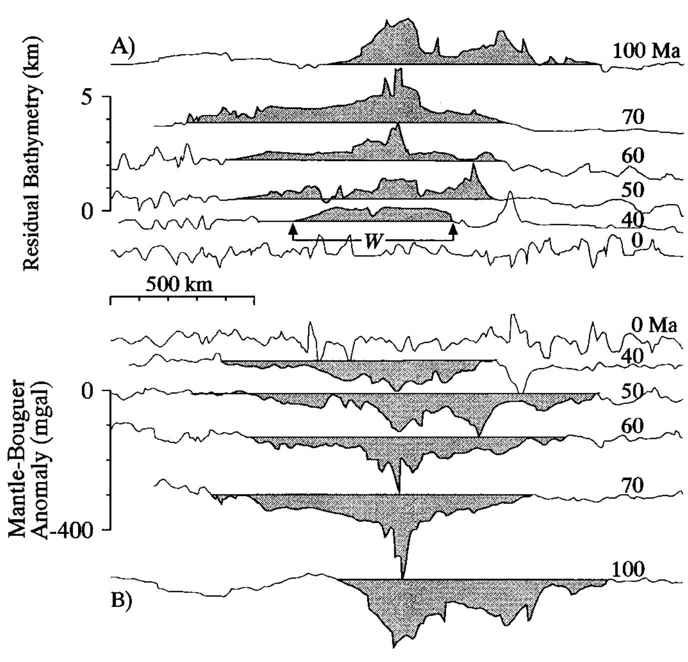

Figure 2. (A) Residual bathymetry (RB) and (B) mantle Bouguer anomaly (MBA) profiles along six example isochrons of Tristan system. Shaded parts mark long-wavelength signals we attribute to hotspots. *W* defines along-isochron width over which long-wavelength topographic swells are shallower than depths predicted by cooling half-space reference model. ΔRB and ΔMBA are maximum amplitudes along each profile. Decrease in amplitudes with decreasing isochron age coincide with migration of Tristan hotspot away from ridge axis since ~80 Ma when it was ridge centered.

The along-isochron variations in residual bathymetric (ΔRB) and mantle Bouguer anomalies (ΔMBA) display a decrease with increasing paleoridge-hotspot distance (D, Fig. 3). The on-ridge hotspot cases (D <50 km) for the Tristan system (80–90 Ma isochrons) and the Iceland system (0–30 Ma isochrons) display the highest ΔRB (3.5–4.7 km) and most negative ΔMBA (−250 to −340 mgal), which are approximately twice those of ridge-centered cases for the Galápagos and Azores systems. At $D \sim 500$ km, the hotspot signals become very weak and in the case of Tristan, become indistinguishable from normal ridge-segmentation–related variations. The individual Galápagos and Tristan systems show a decrease in ΔRB and ΔMBA with increasing D, whereas the Azores system is more complex and the Easter trend is very weak. The predominant decrease of ΔRB and ΔMBA with increasing D is consistent with Schilling's (1985) study of present-day ridge-axis bathymetry.

ANOMALY WIDTHS VS. PALEO–SPREADING RATE

Whereas amplitudes of ΔRB and ΔMBA are functions of ridge-hotspot distance, along-isochron widths (W) of the bathymetric anomalies (see Fig. 2 caption) depend primarily on the full spreading rate (U) at the time of crustal accretion. The maximum values of W are found along the slowest-spreading Mid-Atlantic Ridge near Iceland (2700 km, Fig. 4A); these values are comparable to the along-axis extent of the helium isotope anomaly, but are a factor of two greater than the widths of rare-earth-element anomalies (Schilling, 1986). Values of W decrease with increasing U to a minimum along the fast-spreading East Pacific Rise.

The observed dependence of W on spreading rate lends strong support to previous notions of along-axis plume material flow (Vogt, 1976; Schilling, 1985). Similarly to Schilling (1991), we estimate that the flux of plume material feeding the ridge (Q) is eventually carried away by the spreading lithospheric plates (Fig. 4A, inset), such that

$$Q = \int_{-W/2}^{W/2} P(y)hU\,\mathrm{d}y = \frac{hUW}{2}, \tag{1}$$

where y is the along-axis coordinate, h is the thickness of the fully developed lithosphere (assumed to be 80 km), and $P(y)$ is the percentage of accreted lithosphere derived from the plume material assumed to decrease linearly from 1 at $y = 0$ to 0 at $y = \pm W/2$.

We treat the hotspot to ridge flow as a simple laminar flow problem in which the lithospheric drag opposes the ridgeward flow of plume material. The channel connecting the ridge and hotspot has a characteristic width w_1 and thickness w_2 (see Fig. 4, A and B, insets). Therefore, the net flux from the hotspot to the ridge is

$$Q = w_1 w_2 \left(V - \frac{U}{4} \right), \tag{2}$$

where V is the average ridgeward velocity of plume flow, $w_1 w_2 V$ is the ridgeward flux, and $w_1 w_2 U/4$ is the opposing plate-driven flux. Combining equations 1 and 2 yields the dependence of W on spreading rate,

$$W = \left(\frac{2w_1 w_2}{hU} \right) \left(V - \frac{U}{4} \right). \tag{3}$$

The solid curve in Figure 4A is that predicted for assumed values of V = 70 km/m.y. and $w_1 w_2 = 3 \times 10^4$ km^2, which yields a root-mean-square misfit to the data of 500 km. Similar misfits are achieved for V = 30–100 km/m.y. and corresponding values of $w_1 w_2$ of 8–2 $\times 10^4$ km^2. These results suggest that the ridgeward fluxes from the five

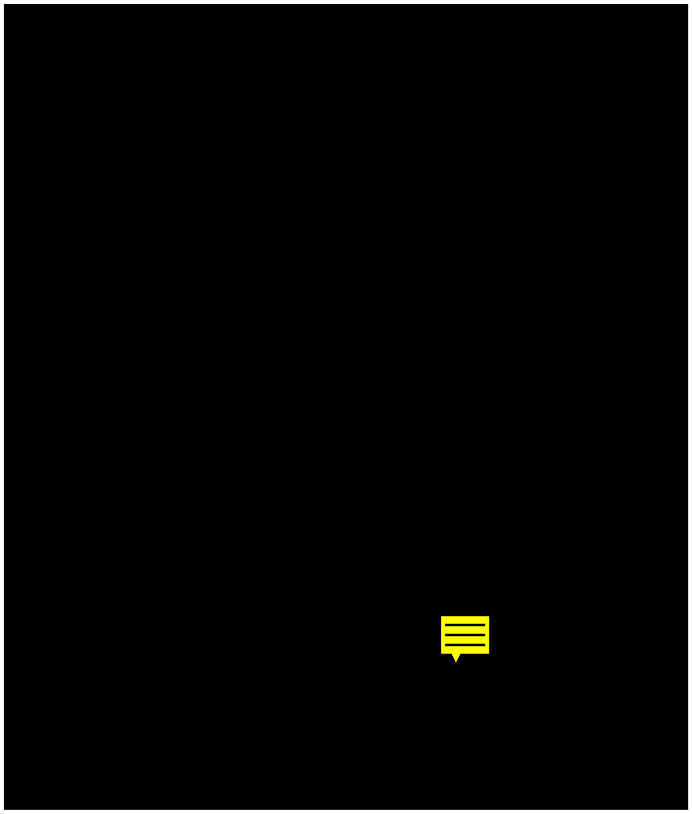

Figure 3. Along-isochron amplitudes of (A) Δ*RB* and (B) Δ*MBA* plotted against distance between paleo–ridge axes and hotspots at times corresponding to isochron ages. Asterisks mark present-day ridge-axis anomalies; solid lines are those that best fit all data. Uncertainties in Δ*RB* and Δ*MBA* are segmentation-scale variations (Lin and Phipps Morgan, 1992) that are independent of larger wavelength hotspot signals. Uncertainties in *D* reflect uncertainties in isochron ages and in plate motion relative to hotspots (Cande and Kent, 1992).

hotspots are comparable, the average value being $\sim 2.2 \times 10^6$ km^3/m.y. Increasing or decreasing $w_1 w_2 V$ by 1×10^6 km^3/m.y. increases the data misfit by a factor of two.

Our theoretical relation between W and U is based on one end-member scenario in which lateral spreading of plume material beneath ridges is strictly ridge parallel. A numerical study that considers both ridge-parallel and ridge-perpendicular spreading of plumes beneath ridges (Feighner et al., 1995) may represent the other end member; it thus predicts that W is proportional to $(Q/U)^{1/2}$ rather than (Q/U), as does our model.

PALEO–RIDGE-AXIS TEMPERATURE ANOMALIES

We show here how the amplitudes of ΔRB and ΔMBA may reflect the temperature anomalies beneath the paleo–ridge axes. We assume that ΔRB and ΔMBA arise from crustal-thickness and mantle-density anomalies, both of which depend on the ridge-axis temperature anomaly at the time of crustal accretion. ΔRB and ΔMBA can be related to a hotspot-induced mantle temperature anomaly (ΔT) using the model of Ito and Lin (1995), which considered changes in mantle density by thermal expansion, and in crustal thickness by increased decompression melting. Assuming passive mantle upwelling, Ito and Lin (1995) imposed temperature anomalies below the melting zone and then combined the effects of crustal-thickness and mantle-density variations to yield theoretical isostatic bathymetric variations and ΔMBA.

Applying this method for ranges of imposed temperature anomalies and model spreading rates, we derive the empirical relations:

$$\Delta T = (0.11U + 35.3)\Delta RB, \tag{4}$$

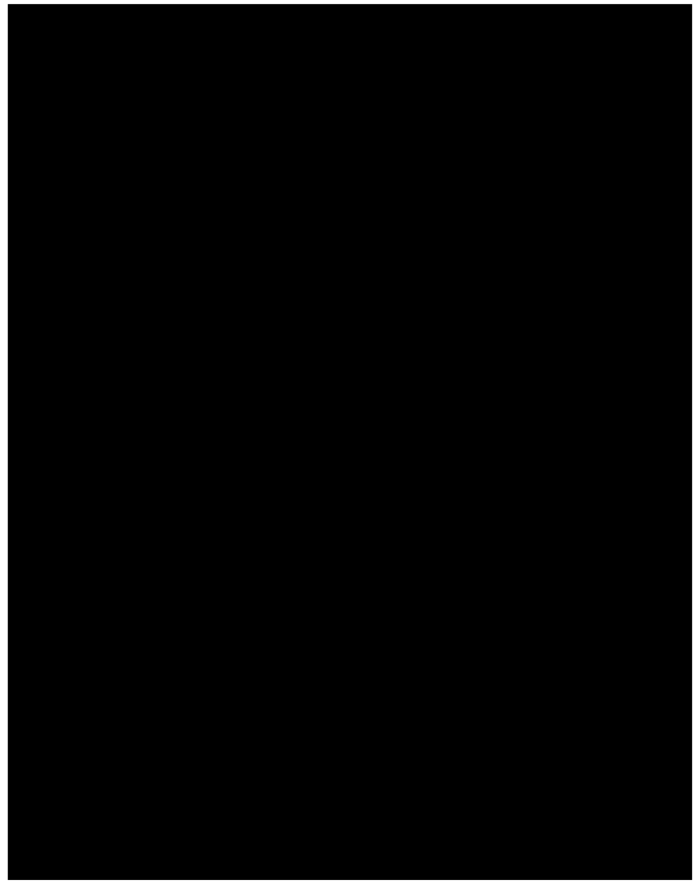

Figure 4. A: Along-isochron widths of residual bathymetric anomalies vs. full spreading rates during times corresponding to isochron ages. Diamonds—Iceland, triangles—Azores, squares—Galápagos, light blue circles—Tristan, dark blue circles—Easter. Asterisks mark present-day ridge-axis anomalies. Present-day spreading rates are from DeMets et al. (1990); paleorates are from Cande and Kent (1992), Mayes et al. (1990), Srivastava and Tapscott (1986), and Wilson and Hey (1995). Note that Iceland, Azores, Galápagos, and Easter plot in tight groupings, each defining narrow range in *W* (≤600 km) and *U* (≤20 km/m.y.). Tristan anomalies encompass wider range in *W*, reflecting secondary dependence on *D* (best fitting line is *W = 1690 − 3.3D;* root-mean-square misfit is 250 km). Solid curve is relation derived in text. Inset illustrates map view of plume-ridge flow pattern; dot pattern marks plume material. B: Along-isochron temperature anomalies (derived from method of Ito and Lin, 1995) plotted against *D.* Solid curve is predicted by conductive cooling. Inset illustrates depth cross section of plume conduit between hotspot and ridge axis.

and

$$\Delta T = -(0.0017U + 0.45)\Delta MBA. \tag{5}$$

The dependence of ΔT on U reflects a subtle dependence of crustal thickness on spreading rate that is consistent with calculations of Su et al. (1994). For $\Delta T = 100$ °C and $U = 20$–100 km/m.y., for example, we predict corresponding values of crustal thickening of 9–4.5 km.

Temperature anomalies derived accordingly from the observed ΔRB and ΔMBA are maximum for the on-ridge cases (150–225 °C), and decrease to near zero for $D \sim 500$ km (Fig. 4B). Such a behavior can be interpreted as the cooling trend of plume material as it migrates from hotspot centers to nearby ridges, the ridge-centered cases reflecting the temperature anomaly of the hotspot itself.

As plume material migrates from a hotspot center to a ridge, it conducts heat to the surrounding mantle (see Fig. 4, A and B, insets). Assuming that the amount of heat conducted in the direction of plume flow is negligible, the heat balance equation is

$$\rho c_p \frac{\partial T}{\partial x} V = -\left(\frac{\partial q_y}{\partial y} + \frac{\partial q_z}{\partial z}\right), \qquad (6)$$

where T is the average temperature of the plume conduit, ρ and c_p are the density and heat capacity of the plume material, respectively, and q_y and q_z are the components of conductive heat flow out of the conduit walls. If we assume that heat loss occurs through a thermal boundary layer surrounding the plume channel with thickness δ,

$$q_z \sim q_y \sim \frac{k\Delta T}{\delta}, \qquad (7)$$

where k is the mantle thermal conductivity (3 W m^{-1} °C^{-1}) and δ is defined such that $q = 30$–100 mW/m^3, comparable to heat-flux values on the sea floor. If it is assumed that the gradients $\partial q_y/\partial y$ and $\partial q_z/\partial z$ are proportional to $1/w_1$ and $1/w_2$, respectively, and $Q \sim w_1 w_2 V$ (i.e., $V \gg U/4$), the combination of equations 6 and 7 yields

$$\frac{\partial T}{\partial x} = -\frac{2\kappa}{Q\delta}(w_1 + w_2)\Delta T, \qquad (8)$$

where $\kappa = k/\rho c_p$ is thermal diffusivity (10^{-6} m^2/s). Integrating with respect to x from 0 to D yields

$$\Delta T = \Delta T_o \exp\left[-\frac{2\kappa}{Q\delta}(w_1 + w_2)D\right], \qquad (9)$$

where ΔT_o is the temperature anomaly at the hotspot center.

Taking $\Delta T_o = 100$ °C, $(w_1 + w_2) = 400$ km, and $Q = 2.2 \times 10^6$ km^3/m.y. as consistent with the observed W vs. U trend above, we produce a theoretical curve (Fig. 4B) that effectively matches the inferred temperature anomalies for $D > 50$ km. For $D \leq 100$ km, the Iceland and Tristan points lie significantly higher than the theoretical curve. This mismatch may be because (1) the Iceland and early Tristan plumes are hotter than the other hotspots and/or (2) latent heat loss due to melting at the hotspot centers rapidly cools the plume before it migrates to nearby ridges in the off-axis cases. For $D \sim 500$ km, ΔT is small enough that its effects on ΔRB and ΔMBA are negligible, even though the plume may still be feeding the ridge. Consequently, the geochemical signal may persist to a ridge-hotspot distance of up to 850 km (Schilling et al., 1985), long after the signals in ΔRB and ΔMBA have disappeared.

CONCLUSIONS

Along-isochron variations in residual bathymetry and mantle Bouguer gravity reflect the influence of hotspots on paleoaxes of nearby spreading centers. The amplitudes of along-isochron anomalies for the five prominent plume-ridge systems reach a maximum of 4.7 km for ΔRB and -340 mgal for ΔMBA and decrease with increasing paleoridge-hotspot distance. The along-isochron widths (0–2700 km), however, depend inversely on paleo–spreading rate. Whereas the widths of ΔRB reflect the balance between ridgeward plume flux and lithospheric accretion, the amplitudes of ΔRB and ΔMBA reflect paleoaxial temperature anomalies that decrease as the plume material cools along its lateral migration to nearby ridges. The five hotspots appear to deliver material to ridges with comparable fluxes of $\sim 2.2 \times 10^6$ km^3/m.y. and produce excess mantle temperature anomalies of 50 to 225 °C that influence ridge-axis structure to a maximum ridge-hotspot distance of ~ 500 km.

ACKNOWLEDGMENTS

Supported by National Science Foundation grant OCE-9302915. We thank Robert Detrick for providing high-resolution bathymetric and gravity data (from near the Azores), and Emilie Hooft, Gary Jaroslow, Deborah Smith, Chris Kincaid, and an anonymous reviewer for constructive reviews of the manuscript. Woods Hole Oceanographic Institution contribution no. 8861.

REFERENCES CITED

Cande, S. C., and Kent, D. V., 1992, A new geomagnetic polarity time scale for the Late Cretaceous and Cenozoic: Journal of Geophysical Research, v. 97, p. 13,917–13,951.

Carlson, R. L., and Johnson, H. P., 1994, On modeling the thermal evolution of the oceanic upper mantle: An assessment of the cooling plate model: Journal of Geophysical Research, v. 99, p. 3201–3214.

DeMets, C., Gordon, R. G., Argus, D. F., and Stein, S., 1990, Current plate motions: Geophysical Journal International, v. 101, p. 425–478.

Feighner, M. A., Kellogg, L. H., and Travis, B. J., 1995, Numerical modeling of chemically buoyant mantle plumes at spreading ridges: Geophysical Research Letters, v. 22, p. 715–718.

Hamelin, B., Dupré, B., and Allègre, C. J., 1984, Lead-strontium isotopic variations along the East Pacific Rise and the Mid-Atlantic Ridge: A comparative study: Earth and Planetary Science Letters, v. 67, p. 340–350.

Hart, S. R., Schilling, J.-G., and Powell, J. L., 1973, Basalts from Iceland and along the Reykjanes Ridge: Sr isotope geochemistry: Nature, Physical Science, v. 246, p. 104–107.

Ito, G., and Lin, J., 1995, Mantle temperature anomalies along the present and paleoaxes of the Galápagos spreading center as inferred from gravity analyses: Journal of Geophysical Research, v. 100, p. 3733–3745.

Kuo, B.-Y., and Forsyth, D. W., 1988, Gravity anomalies of the ridge-transform system in the South Atlantic between 31 and 34.5 °S: Upwelling centers and variations in crustal thickness: Marine Geophysical Research, v. 10, p. 205–232.

Lin, J., and Phipps Morgan, J., 1992, The spreading rate dependence of three-dimensional mid-ocean ridge gravity structure: Geophysical Research Letters, v. 19, p. 13–16.

Lonsdale, P., 1988, Geography and history of the Louisville hotspot chain in the southwest Pacific: Journal of Geophysical Research, v. 93, p. 3078–3104.

Mayes, C. L., Lawver, L. A., and Sandwell, D. T., 1990, Tectonic history and new isochron chart of the South Pacific: Journal of Geophysical Research, v. 95, p. 8543–8567.

Morgan, W. J., 1978, Rodriguez, Darwin, Amsterdam, . . . , A second type of hot spot island: Journal of Geophysical Research, v. 83, p. 5355–5360.

Müller, R. D., Roest, W. R., Royer, J.-Y., Gahagan, L. M., and Sclater, J. G., 1993a, A digital age map of the ocean floor: Scripps Institution of Oceanography Reference Series 93-30.

Müller, R. D., Royer, J.-Y., and Lawver, L. A., 1993b, Revised plate motions relative to the hotspots from combined Atlantic and Indian Ocean hotspot tracks: Geology, v. 21, p. 275–278.

O'Connor, J. M., and Duncan, R. A., 1990, Evolution of the Walvis Ridge–Rio Grande Rise hot spot system: Implications for the African and South American plate motions over plumes: Journal of Geophysical Research, v. 95, p. 17,475–17,502.

Sandwell, D. T., and Smith, W. H., 1992, Global marine gravity from ERS-1, GEOSAT and SEASAT reveals new tectonic fabric [abs.]: Eos (Transactions, American Geophysical Union), v. 73, p. 133.

Schilling, J.-G., 1985, Upper mantle heterogeneities and dynamics: Nature, v. 314, p. 62–67.

Schilling, J.-G., 1986, Geochemical and isotopic variation along the Mid-Atlantic Ridge axis from 79°N to 0°N, *in* Vogt, P. R., and Tucholke, B. E., eds., The western North Atlantic region: Boulder, Colorado, Geological Society of America, Geology of North America, v. M, p. 137–156.

Schilling, J.-G., 1991, Fluxes and excess temperatures of mantle plumes inferred from their interaction with migrating mid-ocean ridges: Nature, v. 352, p. 397–403.

Schilling, J.-G., Thompson, G., Kingsley, R., and Humphris, S., 1985, Hotspot–migrating ridge interaction in the South Atlantic: Nature, v. 313, p. 187–191.

Srivastava, S. P., and Tapscott, C. R., 1986, Plate kinematics of the North Atlantic, *in* Vogt, P. R., and Tucholke, B. E., eds., The western North Atlantic region: Boulder, Colorado, Geological Society of America, Geology of North America, v. M, p. 379–404.

Su, W., Mutter, C. Z., Mutter, J. C., and Buck, W. R., 1994, Some theoretical predictions on the relationships among spreading rate, mantle temperature, and crustal thickness: Journal of Geophysical Research, v. 99, p. 3215–3227.

Vogt, P. R., 1976, Plumes, subaxial pipe flow, and topography along the mid-oceanic ridge: Earth and Planetary Science Letters, v. 29, p. 309–325.

Wilson, D. S., and Hey, R. N., 1995, History of rift propagation and magnetization intensity for the Cocos-Nazca spreading center: Journal of Geophysical Research (in press).

Manuscript received November 14, 1994
Revised manuscript received March 29, 1995
Manuscript accepted April 6, 1995

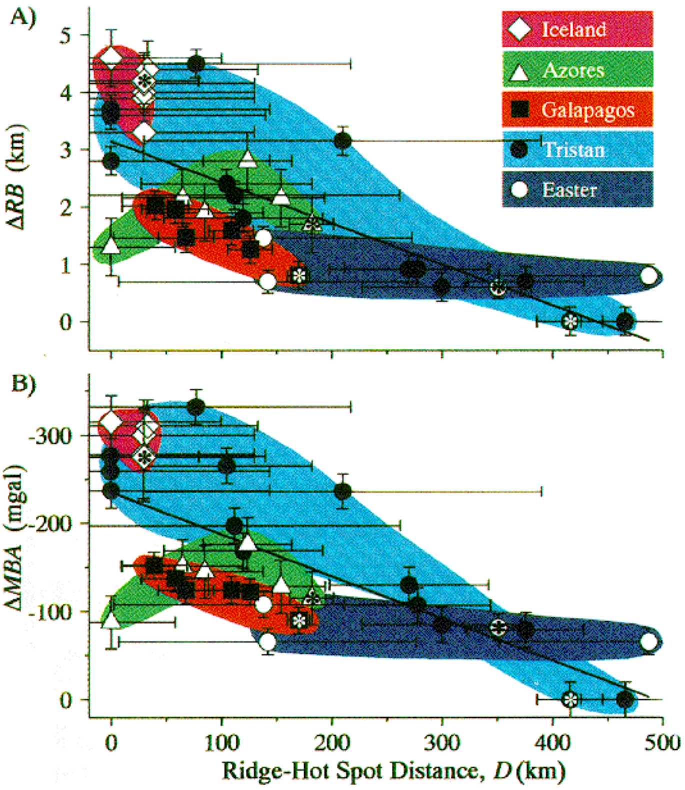

A)
Iceland
Azores
Galapagos
Tristan
Easter
ΔRB (km)
5
4
3
2
1
0
B)
ΔMBA (mgal)
-300
-200
-100
0
0
100
200
300
400
500
Ridge-Hot Spot Distance, D (km)

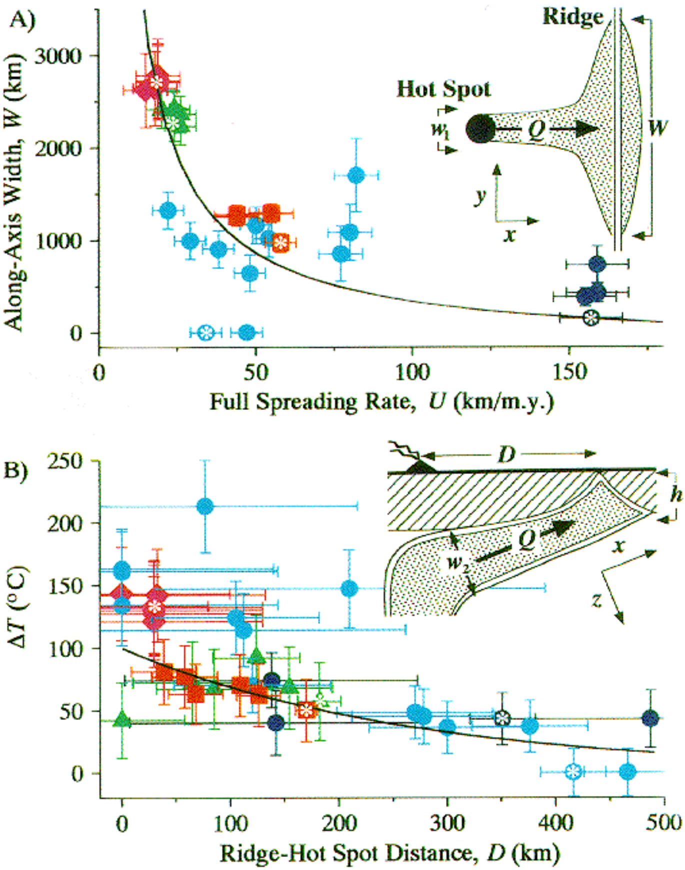

A)
Along-Axis Width, W (km)
3000
2000
1000
0
Ridge
Hot Spot
w_1
Q
W
y
x
0
50
100
150
Full Spreading Rate, U (km/m.y.)
B)
250
200
150
100
50
0
ΔT (°C)
D
h
Q
w_2
x
z
0
100
200
300
400
500
Ridge-Hot Spot Distance, D (km)